IRSTI 29.15.03, 29.15.19 https://doi.org/10.26577/ijmph.20261711

VIRTUAL STATE

Makoto Ito [1] **and Kiyoshi Kato** [2]

[1] *Kansai University, Faculty of Systems Engineering and Science, Osaka, Japan*
[2] *Hokkaido University, Graduate School of Science, Sapporo, Japan*

Email: itomk@kansai-u.ac.jp; kato@nucl.sci.hokudai.ac.jp

(Received 8 April 2026; revised 3 May 2026; accepted 3 June 2026)

Abstract. This review article explains the properties of virtual states and discusses their impact on realistic nuclear structure and nuclear reaction problems. The first half of the paper defines virtual states as poles of the scattering matrix, i.e., zeros of the Jost function, and discusses their similarities and differences with bound and (zero energy) resonant states. The second half of the paper provides concrete examples of the effects of virtual states in real nuclear systems. Regarding nuclear structure problems, we demonstrate the valence neutron occupying virtual state plays important roles in the formation of the anomalous structures in the binary and three-body systems: ^{9}Li + neutron and α + α + neutron. On the other hand, in reaction problems, we address thermal neutron scattering by various targets and discuss the close relationship between the peak structure in the so-called S-wave strength function and the virtual states. By synthesizing the calculation about the neutron scattering, we propose a new reaction picture for thermal neutron absorption reactions.

Keywords: Virtual states, nuclear structure, neutron scattering, neutron capture, nuclear reactions.

1. Introduction

A virtual state can be said to be a state in which a bound state fails to become a resonance state. The existence of a virtual state was first noticed in the low-energy scattering of neutrons and protons [1, 2, 3]. The only bound state in a two-nucleon system is the deuteron, which is the proton-neutron ^3S state. It is known that the ^1S state is not a bound state, but is a state called a virtual state. Recently, the existence of virtual states in several nucleus-neutron systems, not just neutron-proton systems, has attracted attention in connection with the formation of large cross sections near the neutron emission threshold energy (neutron separation energy) and the formation of spatially extended structures such as neutron halo structures near the threshold.

Virtual states are a special state with negative energy that appears only in neutron S-wave scattering in nuclear systems. When it exists near zero energy, it significantly affects the low-energy scattering state. However, it is rarely discussed in standard quantum mechanics or scattering theory textbooks [4, 5]. A concept similar to virtual states is called zero-energy resonance, which is often explained in textbooks [4, 5, 6, 7] and is often confused with virtual states. However, the two are fundamentally different states and should be strictly distinguished. (Incidentally, while zero-energy resonance states are called resonances, their properties differ from the well-known normal resonance states.)

In this article, we focus on virtual states, which have rarely been discussed in detail until now, and explain their properties, particularly their differences from zero-energy resonances and bound states. In addition, we introduce recent researchs on the role of virtual states in nuclear structure and thermal neutron elastic scattering and discuss the role virtual states play in real nuclear systems. We hope this article helps readers deepen their understanding of virtual states.

As an aside, the term virtual state often appears in other fields as well. For example, in the application of perturbation theory, it is well-known that intermediately excited quantum states are often called virtual states. On the other hand, states that are close to bound states but are not strictly eigenstates of the Hamiltonian are also sometimes called virtual states [6]. The term vir-

tual state also appears in reactor physics, which is closely related to nuclear data, but it refers to energy levels that exist in the energy region above the minimum threshold for particle decay [8]. We should add in advance that the virtual state we are attempting to explain here is a special quantum state that is fundamentally different from these terms.

2. WHAT IS A VIRTUAL STATE?

a. Classification of quantum states in complex momentum space

Since scattering states are typically observed over real momentum or energy, various quantum states are often defined over real energy. Resonant states are a typical example [4, 5, 6]. Here, we classify various quantum states, including virtual states, in complex momentum (k) space rather than real energy space [4, 5, 9]. Classification in complex k space is mathematical and somewhat divergent from real scattering phenomena, but it has the great advantage of being able to classify and define quantum states without uncertainty.

To explain the classification of quantum states, we must first discuss the relationship between the Jost function and the scattering matrix (S-matrix). For clarity, we consider a simple neutron one-body potential problem and take the orbital angular momentum of the system to be an S-wave. We also assume that the one-body potential is given by a finite range of attractive forces and real numbers. In this case, the radial solution $rR(r)$ of the Schrodinger equation is known to have the following asymptotic form [6].

$$\lim_{r\to\infty} rR(r) = \frac{i}{2k}\cdot\left\{\mathscr{F}^{(-)}(k)e^{-ikr} - \mathscr{F}^{(+)}(k)e^{+ikr}\right\} \tag{1}$$

Here, r is the radial coordinate of the neutron, and k represents momentum, which is generally a complex number. The amplitudes of the incoming and outgoing waves, $\mathscr{F}^{(\pm)}(k)$, are functions that depend on k and are called Jost functions [4, 6]. The scattering state of a neutron is described by the S-matrix ($S(k)$), where $S(k)$ is given by the ratio of the amplitude of the outgoing wave to the amplitude of the incident wave (incoming wave). Therefore, $S(k)$ can be expressed using the Jost function as follows:

$$S(k) = \frac{\mathscr{F}^{(+)}(k)}{\mathscr{F}^{(-)}(k)} \ . \tag{2}$$

As can be seen from Eq. (2), k_0^+ satisfying $\mathscr{F}^{(+)}(k_0^+) = 0$ represents a zero point of the S-matrix, and k_0^-, which satisfies $\mathscr{F}^{(-)}(k_0^-) = 0$, corresponds to a pole of the S-matrix.

Now, let us consider the behavior of the wave function, Eq. (1), at the latter pole, $k = k_0^-$. In this case, only the outgoing wave component (e^{+ikr}) remains in the wave function, and the boundary conditions of the wave function are uniquely determined. Therefore, the wave function at $k = k_0^-$ corresponds to a quantum state determined by the boundary conditions, and its eigenenergy E is given by $E(k_0^-) = \hbar^2(k_0^-)^2/2\mu$ (where μ is the reduced mass of a neutron). k_0^- takes on various complex values depending on the boundary conditions, and is classified into several quantum states depending on its location on the complex k plane. Figure 1 shows a schematic diagram of the distribution of k_0^- and the corresponding classification of quantum states. [9]

In Fig. 1, the blue and white circles on the imaginary axis (vertical axis) at $k = k_0^-$, i.e., the positive and negative regions on the imaginary axis, correspond to bound states (B.S.) and antibound states (A.B.S.), respectively. Meanwhile, the poles in the fourth and third quadrants, the black and white diamonds, are called resonance states (R.S.) and antiresonance states (A.R.S.), respectively. Virtual states are also classified as poles on the complex k plane, but they have a slightly different character from these quantum states. Let us explain step by step. The arrows in Fig. 1 roughly represent the movement of the poles as the attractive force of the neutron potential is increased. In this case, resonance (R.S.) and antiresonance (A.R.S.) move toward the imaginary axis, eventually colliding at a finite negative coordinate on the imaginary axis (cross). As the attractive force becomes stronger, these two states bifurcate at the cross point on the imaginary

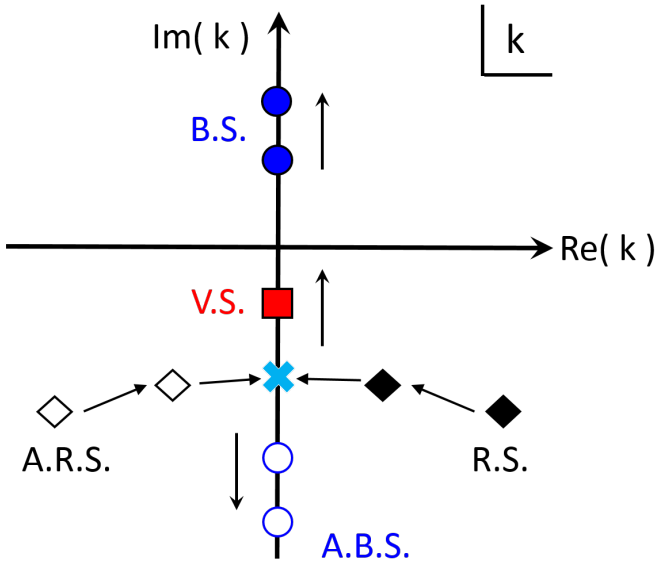

Figure 1 - (Color online) Schematic diagram of the pole distribution of the S-matrix on the complex momentum (k) plane. Consider a one-body potential system of neutrons, where the potential is real and has a finite range of attractive force. We also assume an S-wave state. The horizontal and vertical axes represent the real and imaginary parts of the momentum (wave number k), respectively. The blue and white circles represent the bound state (B.S.) and antibound state (A.B.S.), respectively, while the black and white diamonds represent the resonance state (R.S.) and antiresonance state (A.R.S.), respectively. The arrows indicate the direction of pole movement when the attractive potential is strengthened. The cross mark indicates the collision point of resonance and antiresonance, and the poles (red squares) that exist between the collision point and the origin are virtual states (V.S.). Reprinted from Ref. [9].

axis, evolving into a bound state (B.S.) and an antibound state (A.B.S.). The virtual state (V.S.) refers to a state that exists in the special region between the origin and the collision point (cross) of R.S. and A.R.S. (red square). Therefore, V.S. is possible to exist around the origin $k = 0$ corresponding to the threshold energy but the location of A.B.S. moves to the large negative imaginary point, being far from the threshold, as the potential attraction is more enhanced.

Since both virtual state (red square) and A.B.S. (white circle) exist in the negative region on the imaginary axis, they are often confused, but they must be clearly distinguished. This is because the virtual state (V.S.) is a special state that exists only in S-wave states. It is easy to extend the discussion so far to finite angular momentum states, such as P-waves and D-waves. When this is done, the orbits associated with increasing attractive force shown in Fig. 1 change significantly. The R.S. and A.R.S. move counterclockwise and clockwise, respectively, while colliding at the origin $k = 0$ and eventually bifurcate into B.S. and A.B.S. [9]. In other words, with finite angular momentum, the collision point (cross) moves to the origin, and the virtual state (V.S.) disappears. This is why virtual states are classified as a special state of S-waves.

b. Specificity of S-wave states

So why do virtual states only appear in S-wave states? While it is difficult to definitively answer this question, it is natural to think that they are closely related to the specificity of S-wave states. Typically, when considering the problem of the finite-range attractive potential of neutrons, for finite angular momentum states such as P-waves and D-waves, the Hamiltonian includes not only the attractive potential but also a centrifugal potential arising from kinetic energy. When a centrifugal potential is added to a finite-range

attractive potential, a repulsive barrier is formed near the surface of the attractive potential. This is called the effective barrier, and it has the effect of tightly confining the wave function of the quantum state shown in the system diagram Fig. 1 within the potential region, and particularly acts to stabilize resonant states.

On the other hand, the S-wave state does not have this centrifugal potential, so the wave function is not confined or stabilized by the effective barrier. Instead, confinement occurs due to the reflection of outgoing waves at the potential surface. A finite-range attractive potential always has a surface, and when an outgoing wave traveling from the interior of the system outward is reflected at the potential surface, and the interference between the outgoing wave and the reflected wave increases the amplitude in the potential region, confinement of the wave function occurs. This interference-induced confinement of the wave function within a potential region is a phenomenon unique to S-waves, and its uniqueness may be one of the factors that lead to the formation of a somewhat unusual quantum state known as a virtual state.

c. *Virtual States as Negative Energy Resonance States*

So far, we have classified quantum states as poles of the S-matrix and discussed the unique properties of virtual states. Here, we will compare virtual states (V.S. in Fig. 1) with the well-known bound states (B.S. in Fig. 1) and resonance states (R.S. in Fig. 1). First, comparing bound states and virtual states, they exist in the positive and negative regions on the imaginary axis of the k-plane, respectively, and their momentum is given by the pure imaginary number $k_0^- = \pm i\beta$ $(\beta > 0)$. Recalling the energy equation, $E(k_0^-) \propto (k_0^-)^2 = -\beta^2$, so both have negative real energies. However, from the $k \propto \sqrt{E}$-equation, momentum k is given by a two-valued function of energy E. Therefore, when considered in the complex E-plane, bound states exist in the first Riemann sheet of the E-plane, while virtual states exist in its second sheet. (The upper half of the complex k-plane corresponds to the first sheet of the complex E-plane, and the lower half corresponds to the second sheet, with a cut on the real axis of $E \geq 0$.)

On the other hand, resonance states exist in the lower half of the complex k-plane (the fourth quadrant), which means they exist in the second sheet of the complex E-plane. In other words, virtual states have negative energy, just like bound states, but they share the same energy plane feature of existing in the second Riemann sheet, just like resonance states. Furthermore, if we weaken the attractive potential, the bound state smoothly transforms into a virtual state, following a path in the opposite direction of the arrow in Fig. 1, and ultimately transitions into a resonance state. These facts are the reason why we mentioned at the beginning that "the virtual state may be a bound state that fails to become a resonant state".

However, the properties of resonance states observed in neutron cross section measurements, etc., are fundamentally different from virtual states. Let us consider again the distribution of the poles of the S-matrix on the complex k-plane shown in Fig. 1. Only the region $k \geq 0$ on the real axis of k (the horizontal axis in Fig. 1) can be observed experimentally. The resonance state (R.S.) shown in Fig. 1 exists near the real axis of $k \geq 0$, and is observed as a clear resonance state in measurements only if the real part of the pole momentum $k_0^- = \alpha - i\beta$ $(\alpha, \beta > 0)$ is sufficiently larger than the imaginary part $(\alpha \gg \beta)$. Resonance states result in an increase in the elastic scattering cross section, and if a resonance state consists of an isolated pole, it is known that the increase in the cross section can be well explained by a Breit–Wigner type formula [10, 3]. Since virtual states are equivalent to resonance states in the sense that they are poles of the S-matrix, when they exist near the real axis, i.e., $k = 0$, they will increase the cross section just like resonance states. However, the real energy $Re(E(k_p^0)) \propto \alpha^2 - \beta^2$ of a resonance state is positive, while that of a virtual state is negative, making them different. Since both have the common feature of increasing the cross section, a virtual state could be considered

a negative-energy resonance state. On the other hand, considering virtual states to be on the same level as resonance states can sometimes lead to the misunderstanding that virtual states have positive energy, so it is important to properly distinguish between virtual states and resonance states, including whether their energy is positive or negative. (Incidentally, a detailed explanation of resonance states and terminology can be found in reference [5].)

d. Characteristics of Virtual States: Scattering Length and Phase Shift

We have explained the mathematical definition of virtual states and their comparison with resonant states. Here, we will assume that virtual states exist near $k = 0$ and compare them with zero-energy resonance, which is frequently discussed in textbooks. Zero-energy resonance refers to a situation in which a weakly bound state exists near zero energy. For stricter discussion, we will divide zero-energy resonance into two cases: one in which the absolute value of the binding energy is small but finite, and one in which the energy is exactly zero. The former corresponds to the bound state (B.S.) in Fig. 1 approaching the origin, while the latter will be called the null state (N.S.). As mentioned above, the virtual state increases the cross section. Since the null state (N.S.) and weakly bound state (B.S.) are also poles on the k-plane, if these poles exist, the cross section increases near the corresponding energy, i.e., zero energy. The increase in cross section is a property shared with virtual states.

However, the most significant difference between virtual states and zero-energy resonances is reflected in the scattering length and phase shift. To roughly understand the behavior of the scattering length, we will first consider neutron S-wave scattering again and adopt effective range theory [6, 11]. According to effective range theory, the Jost function $\mathscr{F}^{(-)}$ is given as follows [6]:

$$\mathscr{F}^{(-)}(k) = \frac{k - i\kappa}{k + iC}. \tag{3}$$

Here, κ and C are real numbers, and we assume $C > 0$. The single zero of $\mathscr{F}^{(-)}$, i.e., the pole of the S-matrix, is at $k = i\kappa$, and $|\kappa|$ is very small or exactly zero. $\kappa > 0$ corresponds to a bound state (B.S. in Fig. 1), $\kappa < 0$ corresponds to a virtual state (V.S. in Fig. 1), and $\kappa = 0$ corresponds to a null state (N.S.). Using the Jost function given in Eq. (3), the scattering length a can be calculated in a completely closed-form manner with respect to κ, as follows [6]:

$$\frac{1}{a} = \kappa - \frac{1}{2} r_0 \kappa^2. \tag{4}$$

Here, r_0 is the effective range. When the Jost function is given in Eq. (3), $r_0 = 2/(\kappa + C)$.

When the virtual state exists near the origin, i.e., $|\kappa| \approx 0$ and $\kappa < 0$, the scattering length a is negative and diverges, as can be easily seen from Eq. (4). In fact, it is known that the scattering lengths of the neutron-proton and neutron-neutron ${}^1S$ channels are negative and large [1, 2, 3], and have been confirmed to be virtual states. On the other hand, in the case of a bound state with a pole near the origin where $\kappa > 0$, a is positive and diverges, as can be seen from Eq. (4). Furthermore, it can be seen that the null state where $\kappa = 0$ represents a discontinuity in the scattering length.

Next, we will explain the difference in phase shift. It is known that the phase shift in neutron S-wave scattering monotonically increases with decreasing collision energy, but its behavior when zero energy is reached depends on the nature of the pole present in the vicinity [6]. The phase shift near zero energy can be clearly understood from Levinson's theorem [6]. To review, Levinson's theorem is presented below. For S-waves, the zero-energy ($k = 0$) phase shift $\delta_0(k = 0)$ is as follows:

$$\delta_0(0) = \left(n_0 + \frac{1}{2}\right) \cdot \pi \qquad \text{When there is a null state} \tag{5}$$

$$\delta_0(0) = n_0 \cdot \pi \qquad \text{Otherwise.} \tag{6}$$

Here, n_0 represents the number of bound states for S-waves.

Let us again consider the Eq. (3) that represents the Jost function. When $\kappa > 0$ and the pole is located at the bound state position, there is one bound state, so from Eq. (6), $\delta_0(0) = \pi$. In other words, if there is one bound state, the phase shift increases monotonically as the energy decreases, reaching the value of π at zero energy. On the other hand, if there is a null state ($\kappa = 0$), from Eq. (5), $\delta_0(0) = \pi/2$, so the phase shift also increases monotonically and takes the value of $\pi/2$ at zero energy. When the pole is a virtual state ($\kappa < 0$), there is no bound state, so according to Eq. (6), $\delta_0(0) = 0$. Therefore, as the energy decreases, the phase shift initially increases monotonically, but then peaks somewhere and finally settles to zero at zero energy. As can be seen from these explanations, the behavior of the phase shift near zero energy varies depending on the value of κ. However, since the simple example described here is for a single pole, it should be noted that if there are another n_0 poles in the bound state, the phase shift will increase by $n_0 \cdot \pi$ at zero energy.

Let us also show the behavior of the phase shift and scattering length when a single-level resonance exists near zero energy. Here, we assume that there are no bound states and only an isolated single-level resonance exists near zero energy. Single-level resonances are often described by the Breit–Wigner formula. When only elastic scattering of S-wave neutrons occurs, the phase shift $\delta_r(E)$ and S-matrix $S_r(E)$ near the resonance are given by the formula [3, 5, 10]:

$$\delta_r(E) = -\cot^{-1}\left(\frac{E - E_r}{\Gamma_n/2}\right) \tag{7}$$

$$S_r(E) = \left(1 - \frac{i\Gamma_n}{E - E_r + i\Gamma_n/2}\right) \cdot e^{-2ikR'}. \tag{8}$$

Here, E_r is the energy of the resonance state near zero energy ($E_r \sim 0$), Γ_n is the neutron width, and R' is a radius parameter with a magnitude similar to the nuclear radius [12]. The first term in Eq. (8) represents the contribution from hard sphere scattering, and the second term represents the contribution from resonant scattering.

For the resonance energy ($E = E_r$), from Eq. (7), $\delta(E = E_r) = \pi/2$. Here, the well-known relationship $d\delta_r/dE|_{E=E_r} = 2/\Gamma_n > 0$ [5, 13] is satisfied. If we express the energy dependence of the phase shift by adding the non-resonant contribution (background) to the resonant term in Eq. (7), the phase shift initially increases with decreasing energy. However, as the phase shift approaches the resonance energy E_r, its value rapidly decreases, cutting off $\pi/2$ at $E = E_r$, and the phase shift reaches zero at zero energy (see Levinson's theorem, Eq. (6)).

On the other hand, the scattering length a can be calculated using the following equation:

$$a = \lim_{k\to 0} \frac{-i}{2k}\left[1 - S_r(E)\right] \ . \tag{9}$$

Here, since E_r is close to zero and the condition $E_r \gg \Gamma_n$ holds, we assume that the contribution of the second term (resonance term) in Eq. (8) can be ignored in the limit of $k \to 0$ ($E \to 0$). In fact, experimental data in Ref. [3] shows that this assumption holds well for light target nuclei where neutron absorption and (n,γ) reactions rarely occur. In this case, Eq. (9) can be easily calculated using only the first term in Eq. (8), yielding $a = R'$.

If the second term in Eq. (8) cannot be ignored, the scattering length generally becomes a complex number. In this case, it means that the neutron absorption reaction, the (n,γ) reaction, occurs simultaneously with elastic scattering, and the effect of the γ-ray emission width Γ_γ is added to Eq. (8). It is known that, particularly for nuclei that strongly absorb neutrons, the imaginary part of the scattering length increases with a negative sign (because the imaginary part of the scattering length is directly proportional to the neutron absorption cross section) [11, 14, 15].

The scattering length and phase shift values discussed so far are summarized in Table 1. It should be emphasized that the results in Table 1 are for cases where only S-wave neutron elastic scattering occurs, and the S-matrix has only one pole.

One may consider that the anti-bound state

Region of κ, E_r	$\kappa < 0$	$\kappa = 0$	$\kappa > 0$	$E_r \sim 0$
Quantum state	V.S.	N.S.	B.S.	R.S.
Scattering length	$-\infty$	Discontinuity	$+\infty$	R'
Phase shift	0	$\pi/2$	π	0

Table 1 – Summary of quantum states of S-wave neutrons and the corresponding scattering lengths and phase shifts. The first line shows the sign of κ in Eq. (3) and the resonance energy E_r in Eq. (8). The second line shows the type of quantum state (pole): V.S. stands for virtual state, N.S. for null state, B.S. for bound state, and R.S. for resonant state. The third line shows the scattering length, and the fourth line shows the value of the phase shift at zero energy, with R' representing the radius parameter included in Eq. (8).

(A.B.S. in Fig. 1) affects the scattering length and the phase shift because it is the pole located on the imaginary axis, which is the similar situation to the virtual and bound states. In the S-wave scattering around the zero energy, however, A.B.S. cannot contribute to the scattering cross section becaues of its pole location far from the origin $k = 0$. In the case of the non S-wave scattering, the pole of A.B.S. can be close to the threshold, zero energy, and A.B.S. seems to affect the scattering cross section in the non S-wave scattering (See discussion in Sec. a). However, the finite partial waves themself do not contribute to the scattering process around the zero energy. Thus, A.B.S. is difficult to contribute to the scattering cross section around the zero energy, and we can exclude the discussion about the effect of A.B.S. on the scattering observables from Table 1.

3. JOST FUNCTION METHOD (JFM)

In the previous sections, we have explained virtual states based on the validity of the Jost function and its zeros, i.e., the properties of the poles of the S-matrix. To actually identify the poles in the complex k-plane for a real system, one must typically numerically solve the Schrodinger equation in complex k-space and calculate the Jost function from there. However, by using a technique called the Jost Function Method (JFM) [9, 16], it is possible to calculate the Jost function directly without going through a wave function.

The JFM can be briefly described as follows: To recap, the Jost function is the amplitude of each wave function when it is expressed as a superposition of incoming and outgoing waves in the asymptotic region, as shown in Eq. (1). In JFM, the radial wave function, which is the exact solution to the Schrodinger equation, is expressed as a superposition of incoming and outgoing waves, which is the similar manner to Eq. (1), and a first-order differential equation is derived in which the amplitude of each wave function is an undetermined function. By numerically solving this differential equation, the undetermined function (amplitudes of the outgoing and incoming waves) is naturally connected to the Jost function. For details on JFM, see Refs. [9, 16]. JFM is capable of calculating the poles of any type of quantum state, including virtual states, for general two-body scattering problems, making it an extremely advantageous computational method.

4. VIRTUAL STATES SEEN IN NUCLEAR STRUCTURE

a. ^{9}*Li* + *n system*

For the halo structure of ^{11}Li, Thompson and Zhukov [17] discussed that an s-wave[1] component is important in the halo state for solving the under-binding problem. They suggested that a low-lying virtual$s$-state in the ^{9}Li + n subsystem (^{10}Li) of the ^{9}Li + n + n system (^{11}Li) is necessary to explain the mechanism for the s-wave component in ^{11}Li. However, we encounter a problem why such the s-state comes down to the p-shell energy region in the light nuclei. In

[1] In the shell model for nuclear systems,the orbital angular momenta of the single-particle states are described usually with small letters like s, p, $\cdots$.

the study of the ^{9}Li–n interaction, Katō *et al.* [18] discussed the importance of dynamical effects induced by a Pauli-blocking for a pairing-correlation in the ^{9}Li–core. They showed that the Pauli-blocking gives rise to a strong repulsive effect for the $0p_{1/2}$-orbital, and that the $1s_{1/2}$-orbital could be expected in the same energy region of the $0p_{1/2}$-orbital. This analysis exploits a theoretical understanding of the low-lying 1s-states in the ^{9}Li + n system [18]. A similar effect was also discussed in the Be-isotopes by Sagawa et al. [19].

Masui *et al.* applied the Jost function method [16] to investigate in detail the properties of the s-wave poles of the ^{9}Li + n system using the ^{9}Li–n interaction including the dynamical Pauli-blocking effects. The obtained results of the s-wave pole behavior are shown in Fig. 2. We can see that the original potential ($\delta = 0$) gives the virtual state pole just below zero on the momentum plane and at the very small negative energy on the energy plain.

Such a virtual state of s-waves has been shown to play an important role in the formation of the halo structure in ^{11}Li. Furthermore, Myo *et al.* [20] investigted the Puali blocking effects due to tensor force correlations in addition to the pairing correlations.

b. ^{8}*Be* + *n system*

As another example of a virtual state appearing in nuclear structure, we will introduce the study of the ^{9}Be nucleus. Observed energy levels of ^{9}Be [21] reveal that $1/2^+$ exists as the first excited state just above the ground state ($3/2^-$). This excited state, located just above the threshold of ^{8}Be + n, has long been the subject of debate as to whether it is a resonance or a virtual state. As we have pointed out, the virtual state itself exists in the negative energy region but it generates a prominent peak for a cross section in the positive energy region just above the particle threshold because of its close location to the threshold, zero energy. Thus, experimentally, the enhanced peak observed in the positive energy region is assigned to a special state originating from the virtual state.

The ^{8}Be nucleus, with one less neutron, is known to be in a resonance state of two α clusters, and the structure of the ^{9}Be nucleus needs to be investigated using the $\alpha + \alpha + n$ three-body model. Here, we present the results of Odsuren *et al.*'s $\alpha + \alpha + n$ three-body calculations, which argued that the $1/2^+$ state is a virtual state of ^{8}Be + n [22].

To describe the virtual state of ^{8}Be + n, since ^{8}Be is a resonant state of $\alpha + \alpha$, it is necessary to simultaneously solve the bound, scattering and resonance states of the $\alpha + \alpha + n$ three-body system. Odsuren *et al.* solved this problem using the complex coordinate scaling method (CSM) [23]. However, in CSM, since virtual states cannot be solved as isolated poles, it is difficult to drow a pole-trajectory like those shown in Fig.2. Therefore, they investigated the photodisintegration reaction cross-section observed just above the threshold and confirmed that this large cross-section originates from the virtual state.

In recent years, precise observations [24] of the reverse photodisintegration cross-section have been performed, and the results in the low-energy region, along with theoretical predictions, are shown in Fig.3. The observed cross sections are well reproduced, except for a very sharp peak at $E_x = 2.43$ MeV ($5/2^-$), with the lowest peak just above the ^{8}Be + n threshold corresponding to the $1/2^+$ state. Looking at the contribution of each excited state in Fig.3 (B), we can see that very narrow state ($5/2^-$) is difficult to observe experimentally, but relatively wide resonance states ($1/2^-$ and $5/2^+$) exhibit the Breit-Wigner distribution. The $1/2^+$ peak, which deviates from the Breit-Wigner distribution and exhibits an asymmetric cross-section, suggests that it is a virtual state rather than a normal resonance state. Detailed analysis [25] confirmed that the calculated $1/2^+$ state is indeed a virtual state.

Thus, it has become clear that the virtual state results in a large neutron capture cross-section just above the neutron emission threshold. If virtual states exist in other atomic nuclei as well, large neutron capture cross-sections are expected, and these are anticipated to play an im-

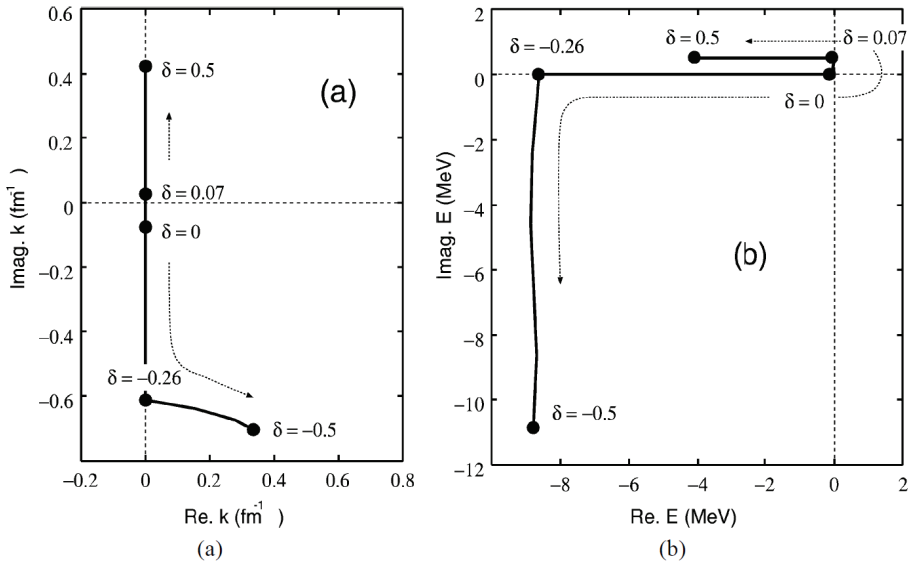

Figure 2 - Behavior of the 1s-pole of the S-matrix for the ^{9}Li$-n$ system is shown on (a) the momentum and (b) the energy planes, respectively. (1+δ) is a parameter of the strength of the potentiall. In the energy plane, the bound state pole is on the first-Riemann sheet and the virtual and resonance poles are on the second - Riemann sheet. Hence, we slightly shift the bound state pole to the positive-imaginary direction, in order to see clearly the behavior of the pole. (Taken from Ref.[16].)

portant role in the nucleosynthesis process. Research into the contribution of virtual states to the nucleosynthesis process is an interesting topic for the future.

The virtual state has a negative energy, but it is not a bound state, so it is not shown in the calculation results of the energy levels in Fig.3 (C). However, it is expected that a miror state in the ^{9}B nucleus can be observed as a resonant state. Because the valence neutron in the ^{8}Be + n virtual state is replaced by a proton in the ^{9}B nucleus, the Coulomb intercation between the proton and the ^{8}Be core makes a barrier. The virtual state has negative energy, but it is not written as a bound state in the calculation results of the energy levels in Fig.3 (C). On the other hand, it is expected that a mirror state corresponding to the ^{9}Be virtual state will be observed as a resonant state in the ^{9}B nucleus. This is because the valence neutron in the ^{8}Be + n virtual state is replaced by a proton in the ^{9}B nucleus, and the Coulomb interaction between the proton and the ^{8}Be core is thought to form a barrier that prevents particle emission and creates a resonant state.

According to Odsuren et al.'s three-body calculation of $\alpha+\alpha+p$ for ^{9}B, in addition to the $1/2^+$ resonance state at $E^{res} = 1.81$ MeV measured from the $\alpha+\alpha+p$ threshold, another resonance state is predicted at a very close energy $E^{res} = 2.38$ MeV [22]. These results suggest the breaking of the mirror symmetry in the virtual state due to a large effect of the Coulomb interaction.

5. Virtual States in Thermal Neutron Scattering

a. S-Wave Neutron Strength Function

In Section 2, we looked at various aspects of the properties of virtual states. In addition, the effects of the virtual state on the nuclear structure aspect were discussed in Section 4. Returning to the well-known scattering of thermal neutrons with various atomic nuclei, we notice the potential for virtual state effects. In fact, the S-wave neutron strength function $S_0 = \Gamma_n/D$ (where Γ_n is the neutron width and D is the mean level spacing) in the thermal neutron energy region, or the thermal neutron compound nucleus formation cross section $\sigma_{CN} = 2\pi^2/k^2 \cdot S_0$, exhibits a pro-

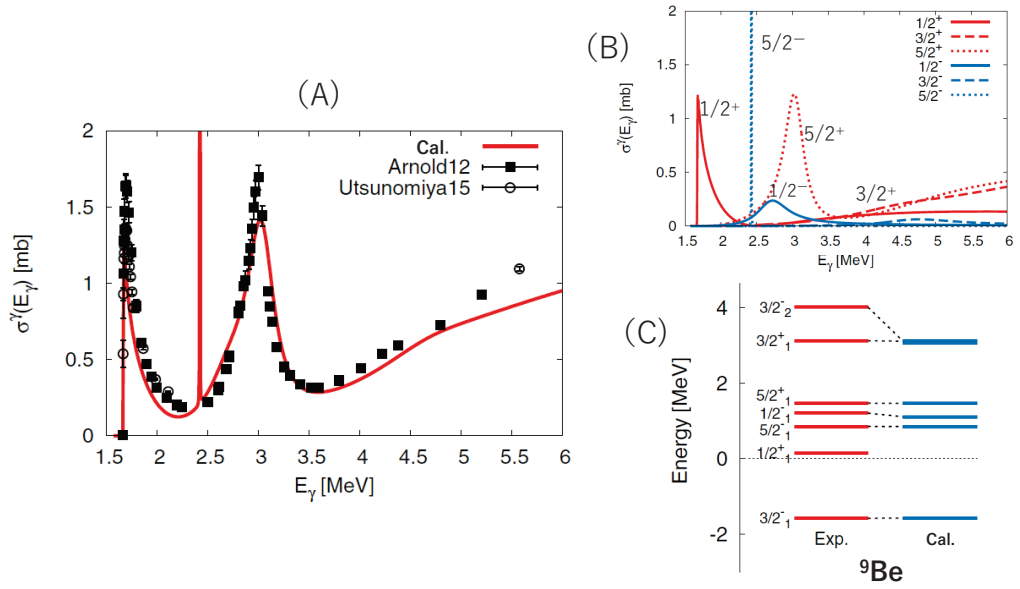

Figure 3 - (Color online) (A) Calculated photodisintegration cross sections of ^{9}Be in comparison with the experimental data [26]. (B) Contributions from each spin-parity state to the photodisintegration cross section. (C) Enegy levels of ^{9}Be, The experimental data are taken from Ref.[21]. (Taken from Ref.[27].)

nounced peak structure in a specific mass number region. As discussed below, optical model analysis has argued that this peak structure is due to the presence of zero-energy resonances [28, 29]. H. A. Weidenmuller pointed out that this zero-energy resonance is actually a virtual state. (See, for example, Ref. [30]).

To examine the effect of the virtual state on thermal neutron elastic scattering, a new reanalysis using the optical model was performed by Yamaguchi *et al.* [9]. In this reanalysis, the same spherical Woods-Saxon potential as in previous studies was used as the optical potential, but it was extended to include proton and neutron number dependence [28]. The parameter set for the optical potential was determined to qualitatively reproduce the increasing trend in the compound nucleus formation cross section in the $A \sim 10,\ 160$ region.

The results of the S-wave neutron strength function calculations using the optical model are shown in Fig. 4, which is calculated by Okada and Yamaguchi. The theoretical calculation (open circles) shows peak structures in the mass number region $A \sim 10, 50, 160$ (arrows), which correspond well with the experimental data (solid lines with error bars) [29]. This is consistent with previous research, and similar peaks have been obtained in calculations using the optical model shown in Refs. [28, 29]. In other words, it is a universal fact that peaks appear in the three mass number regions as long as a standard optical model is used.

b. Analysis of S-Matrix Poles Using JFM

Next, Yamaguchi *et al.* investigated the distribution of S-matrix poles in the complex momentum (k) plane using the JFM (Jost Function Method) described in section 3 [9]. Specifically, they applied JFM to the entire mass number region, and in particular, investigated the S-matrix poles near the origin (zero energy) of the k plane (points satisfying $\mathscr{F}^{(-)}(k_0^-) = 0$ in Eq. (2)). To simplify the analysis, Yamaguchi *et al.* used only the real part of the optical potential to identify the poles. Figure 5 shows the results of calculations [9]. The solid circles (left axis) represent the calculated thermal neutron compound nucleation cross section ($\sigma_{CN} = 2\pi^2/k^2 \cdot S_0$), and the other symbols represent the poles of the S-matrix found near zero energy. The open triangles, open circles, and open squares represent resonant states,

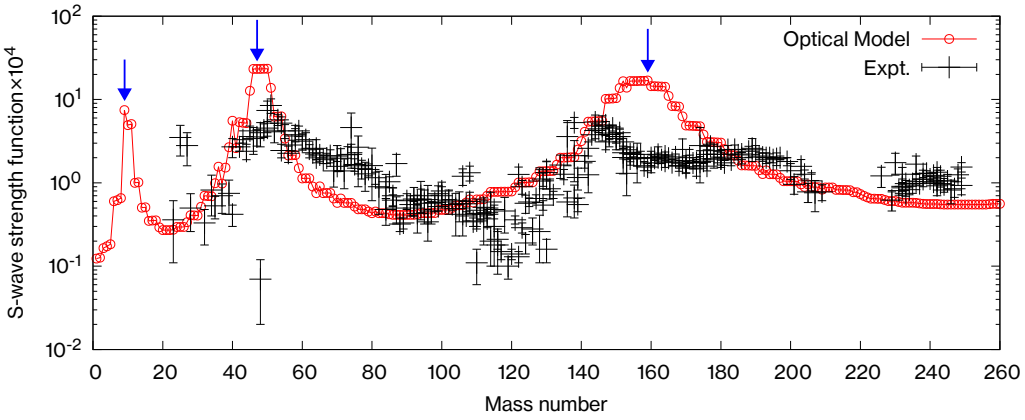

Figure 4 - (Color online) Comparison of experimental and theoretical S-wave neutron strength functions. Open circles represent calculated results using the optical model, and horizontal lines with error bars represent experimental data. The horizontal axis represents mass number, and the vertical axis represents the strength function, $S_0 \times \sqrt{E_0/E_n}$ ($S_0 = \Gamma_n/D$, $E_n = 0.0253$ eV, $E_0 = 1$ eV). The arrows indicate the peak positions of the strength function, corresponding to the boundary between the virtual state and the bound state (see Fig. 5).

bound states, and virtual states, respectively, and the reciprocals of their absolute energy values $|E_0|$, $1/|E_0|$, are plotted on the right axis.

Looking at Fig. 5, the three peaks in the S-wave neutron strength function shown in Fig. 4 are in the same mass number region, i.e., $A \sim 10, 50, 160$. A peak in the compound nucleation cross section (solid circles) is observed in the $A \sim 10, 50, 160$ region, which corresponds to the boundary region between the virtual state (open squares) and the bound state (open circles). Normally, the optical potential exhibits an increasing attractive force as the mass number increases. Therefore, by reading Fig. 4 from left to right, we can see that the three peaks are formed by a periodic, continuous transition from the virtual state to the bound state as the attractive force increases.

This continuous transition is the same behavior as that shown in the explanation of Fig. 1 above. Figure 1 shows how the virtual state smoothly transitions to the bound state as the attractive force increases. The connection between the open squares and circles in Fig. 5 represents this exact transition. In other words, the boundary region at $A \sim 10, 50, 160$, the pole approaches zero energy ($1/|E_0|$ increases), which results in an increase in the cross section. We can conclude that the peaks at $A \sim 10, 50, 160$ are due to the mass number region corresponding to the boundary region between the virtual state and the bound state.

Here, we will discuss in more detail a comparison with previous research using the optical model. In previous research, the zero-energy level [28] or giant resonance [29] was proposed as the origin of the peak in the S-wave neutron strength function. The former literally describes a situation in which a weakly bound state appears near zero energy [28]. On the other hand, giant resonance basically refers to a one-neutron resonance state within the well-shaped potential created by the target nucleus, and its formation at zero energy explains the peak in the strength function [29]. In other words, these two concepts are essentially zero-energy resonances in which a weakly bound state (or null state) is formed near zero energy.

Based on the mass-number dependence of the optical potential, for example, the reference [28] points out that 3s and 4s neutron orbitals appear near zero energy for $A \sim 50$ and $A \sim 160$, respectively. Looking at the lighter region, the neutron-proton ^1S scattering mentioned at the beginning can be considered to correspond to the 1s zero-energy orbital, while the S-wave strength function peak in the $A \sim 10$ region corresponds

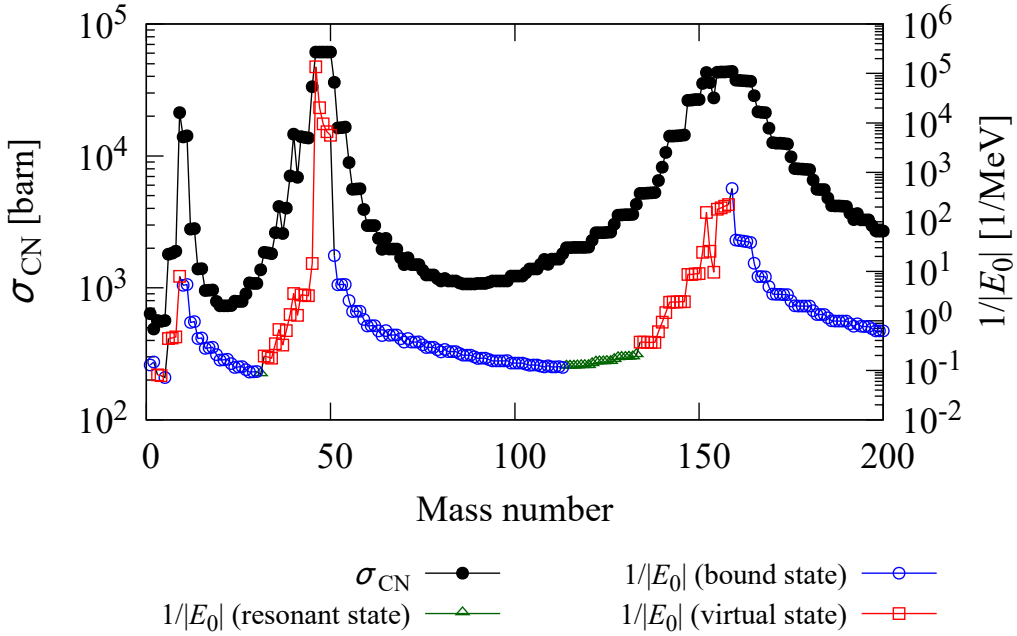

Figure 5 - (Color online) Correlation diagram between thermal neutron compound nucleus formation cross section and zero-energy pole. The solid circles represent the calculated compound nucleus formation cross section ($\sigma_{CN} = 2\pi^2/k^2 \cdot S_0$) and correspond to the left axis. The other symbols represent the reciprocal of the absolute value of the energy (E_0) of the pole closest to zero energy, $1/|E_0|$, and correspond to the right axis. The symbols represent the resonance state (open triangle), the bound state (open circle), and the virtual state (open square). The horizontal axis represents the mass number. Reprinted from Ref. [9].

to the 2s orbital [29]. The results obtained in the present reanalysis suggest that the systematics of these zero-energy orbitals can be interpreted in a new way as a periodic manifestation in the boundary region between the virtual state and the bound state.

c. Fitting analysis of total cross sections taking into account compound nuclear resonances

So far, we have discussed the results of analyses using the optical model + JFM. However, for a more detailed comparison with actual experimental data, optical model analysis alone is insufficient. This is because compound nuclear resonances exist near zero energy, where the neutron energy is dispersed throughout the target nucleus, forming a long-lived state after the neutron is absorbed into the imaginary part of the optical potential. The effect of neutron absorption due to compound nuclear resonances becomes significant in the heavier mass region of $A \sim 160$ [31]. Therefore, Okada *et al.* conducted a more advanced analysis to incorporate the effect of compound nuclear resonances [14].

Specifically, they decompose the total S-matrix (S_{tot}) for thermal neutron elastic scattering into two processes as follows [32]:

$$S_{tot} = S_{VS} + S_{CNR}. \tag{10}$$

The first term on the right-hand side is the elastic scattering (shape elastic scattering) due to the optical potential that occurs in the early stages of the reaction, representing the contribution of the virtual state (VS) discussed so far. Meanwhile, the second term is the contribution from the final state of the reaction resulting from the so-called compound nuclear resonance (CNR) (compound nuclear scattering), which is usually given by the Breit-Wigner resonance formula (the second term in Eq. (8)) [3, 10]. The timescales of the two are significantly different. S_{VS} is the contribution from potential scattering, so it corresponds to the

process in which neutrons collide with the target nucleus and immediately finish scattering. The second term corresponds to the process in which neutrons are absorbed, trapped within the nucleus for a long time, and then released again.

For S_{VS}, which includes the virtual state in the first term of Eq. (10), Okada *et al.* developed a formulation that extends the Jost function of Eq.(3) used in the theory of effective range [11]. Meanwhile, for S_{CNR}, the compound nuclear resonance portion, the Breit–Wigner type formula that takes into accouont the γ-ray width Γ_γ to the second term of Eq. (10) is used. By combining these two terms, they devised a hybrid formula for S_{VS} and S_{CNR} shown in Eq. (10) [14]. Next, using the resulting formula, Okada and Yamaguchi performed a fitting analysis of the total cross sections of the nuclei, which strongly absorb thermal neutrons, and quantitatively evaluated the contributions of the virtual state (VS) and compound nuclear resonance (CNR) [14].

Since Okada-Yamaguchi formula is expected to be appropriate for the nucleus having the huge neutron absorption cross section and the large imaginary part of the scattering length, the mass number of $A \sim 10, 50$ and 160, which correspond to the three peaks in the strength function (Fig. 4) and the compound nucleus formation cross section (Fig. 5), are the candidate of the fitting analyses of the formula. From experimental data [15, 31], we can easily find ^{10}B and (^{149}Sm and ^{157}Gd) as the candidate of $A \sim 10$ and $A \sim 160$, respectively because these nuclei have the huge cross section of the neutron absorption and the large imaginary part of the scattering length.

However, it is difficult to have appropriate nuclei around $A \sim 50$, which should have a large absorption cross section and imaginary part of the scattering length. For example, we can choose ^{50}V as such the candidate for the fitting analyses. This nuleus has the considerably enhanced absorption cross section ($\sigma_a \sim 60$ b) but only the real part of its scattering length is measured, such as $a \sim 7.6$ fm [15]. Thus, Okada and Yamaguchi have excluded the $A \sim 50$ nucleus and performed the fitting analyses for ^{10}B, ^{149}Sm and ^{157}Gd, which have the huge neutron absorption and the large imaginary part of the scattering length.

Figure 6 shows the analysis results for ^{149}Sm [14]. The solid line represents the first term of Eq. (10), the dashed line represents the second term, and the dotted line represents the total contribution. The experimental data for the total cross section are shown as open circles and squares [33, 34]. The experimental data reveals a peak due to the compound nuclear resonance at around $E_n \sim 10^{-1}$ eV, which increases the total cross section in the zero-energy region. On the other hand, we can see that several typical compound-nuclear resonances appear in the $E_n \geq 3 \times 10^{-1}$ eV region.

The calculation results (dotted line) using the full S matrix (S_{tot}) accurately reproduce the total cross section across the entire energy region. Furthermore, while the contribution from the compound-nuclear resonance S_{CNR} (dashed line) is dominant in the low-energy region, above $E_n \sim 3 \times 10^{-1}$ eV, the contribution from S_{VS} (solid line) becomes dominant, exerting a contribution comparable to the approximate average value of the compound-nuclear resonances seen in this region. Focusing on the cross section near zero energy, we can see that the contribution from the virtual state (solid line) is approximately 10 % of the total cross section (dotted line).

Let us review the results obtained here in terms of the reaction timescale. Because ^{149}Sm strongly absorbs thermal neutrons and then emits γ rays, the cross section for the (n,γ) reaction accounts for most of the total cross section shown in Fig. 6 [31]. Therefore, we can conclude that approximately 10 % of the (n,γ) reaction cross section near zero energy is due to the short-timescale component that occurs during scattering by the optical potential at the initial stage of the reaction, i.e., the formation of a virtual state.

d. Scattering Length and Thermal Neutron Reaction Picture

Furthermore, to explore the thermal neutron reaction mechanism in more detail, Okada *et al.* calculated the scattering length [14]. As ex-

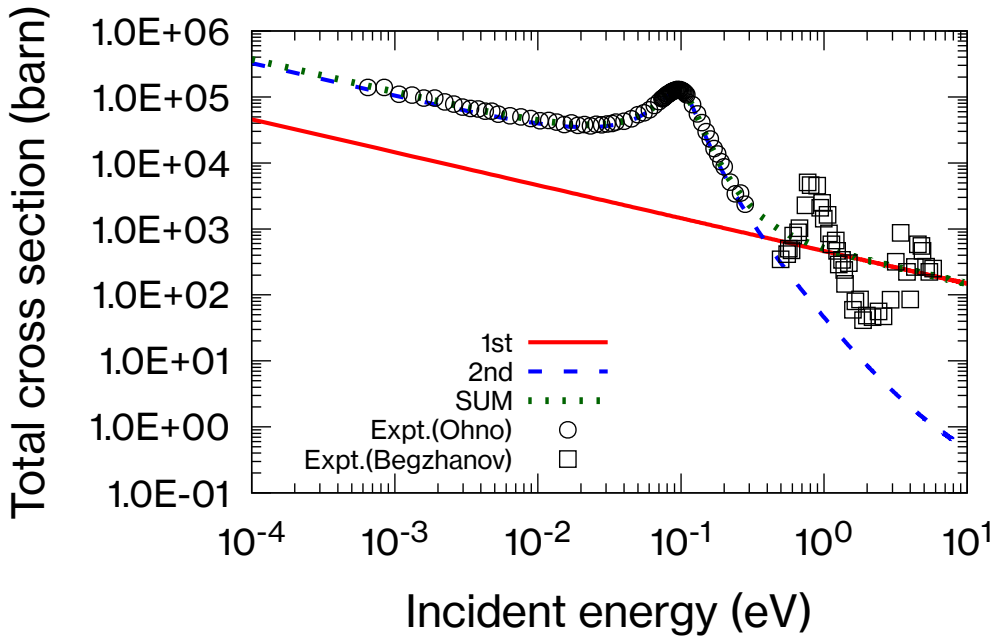

Figure 6 - (Color online) Fitting analysis results for ^{149}Sm. The solid line represents the contribution from the first term, S_{VS}, in Eq. (10), the dashed line represents the contribution from the second term, S_{CNR}, and the dotted line represents the calculated value, S_{tot}, which is the sum of the two terms. The open circles [33] and open squares [34] represent experimental data. The horizontal axis represents the incident neutron energy, and the vertical axis represents the total cross section. Reprinted from Ref. [14].

plained previously, the scattering length a generated by the virtual state diverges as a negative real number, but this only applies when the potential is real and the effect of neutron absorption is absent. As mentioned in Section d, if neutron absorption is involved, the scattering length a becomes a complex number, and the imaginary part of a increases, especially for nuclides that strongly absorb thermal neutrons [14, 15]. The experimental scattering length for ^{149}Sm (a_{exp}) is $a_{exp} = -19.2 - 11.7i$ fm [15], and because it strongly absorbs neutrons, the scattering length has a negative and increased imaginary part (here, the experimental value refers to the bound coherent scattering length found in Ref. [15].). The scattering length (a_{fit}) obtained from the fitting analysis shown in Fig. 6 is $a_{fit} = -19.2 - 10.5i$ fm, which closely reproduces the experimental data. Of these, the contribution ($\Im(a_{VS})$) from the S-matrix S_{VS}, which includes the virtual state, was found to be $\Im(a_{VS}) \approx -1$ fm. The virtual state contribution, $\Im(a_{VS}) \approx -1$ fm, is approximately 10% of the imaginary part of the total scattering length. However, considering that the nuclear radius is on the order of a few fm, the contribution of -1 fm is by no means small and can be said to be significant. This scattering length of -1 fm has also been obtained in fitting analyses of other ^{10}B and ^{157}Gd.

Combining all the results of our analysis, a new reaction picture based on scattering lengths for nuclei that strongly absorb thermal neutrons is established, as follows:

1. In the initial stage of a thermal neutron incident on a target nucleus, scattering by the optical potential (contribution from S_{VS}) occurs first, forming a virtual state.

2. Next, the neutron in the virtual state undergoes multiple interactions with nucleons within the target nucleus and is absorbed by the target nucleus, generating an imaginary part of the scattering length of approximately -1 fm.

3. The neutron absorbed by the target nucleus scatters its kinetic energy among the nucleons within the target nucleus, eventually forming a compound nuclear resonance.

4. When the compound nucleus reaches the end of its life and decays, re-scattering with the residual nucleus occurs, resulting in the re-absorption of the neutron. This process generates the imaginary part of the remaining scattering length (contribution from S_{CNR}). Of course, in light nuclei where compound nuclear resonances are not significant, such as ^{10}B, the total scattering length is formed simply by passing through the virtual state.

This is the reaction picture of thermal neutrons when virtual states are taken into account.

6. Conclusion

In this article, we provide an overview of the characteristics of virtual states, and explain commonly misunderstood aspects through similarities and differences with resonance states and comparisons with zero-energy resonances. When the potential of the system is real, virtual states have negative energy, and their scattering lengths are negative and divergent, resulting in an increased cross section. These characteristics should be distinguished from ordinary resonance states and zero-energy resonances. Although it is beyond the scope of this paper and cannot be explained in detail, the behavior of the poles of the S-matrix when the potential is complex has also been analyzed by Okada *et al.* and Kawai *et al.*. For more details, please refer to Refs. [11, 14, 35].

As examples of the virtual states in realistic nuclear structure, we showed two systems: ^{9}Li + n [16] and ^{8}Be + n [22]. As for the ^{9}Li + n, the virtual state and its trajectories are calculated from the ^{9}Li–n potential including the dynamical Pauli blocking effects. In the normal strength of the potential, the virtual state appears at the energy quite close to zero energy, and it plays important roles of the degeneracy between the $0p_{1/2}$ and $1s$ orbits, which is essential in the three-body halo formation in ^{11}Li. In the ^{8}Be + n system, on the other hand, the three-body calculation with $\alpha + \alpha + n$ was performed, and the virtual state appears around the three-body threshold with a characteristic asymmetric shape, deviating from the typical Briet-Wigner formula, in the strength of the Coulomb breakup reaction. As seen in these two examples, the virtual state strongly affects on the nuclear structure aspects in the light systems, such as the halo formation and the strength distribution of the photodisintegration.

Furthermore, we have introduced a recent reanalysis of thermal neutron elastic scattering and its relationship to the virtual state [9]. The peak in the mass number region $A \sim 10, 50, 160$ that appears in the S-wave neutron strength function obtained using the optical model corresponds exactly to the boundary region between the virtual state and the bound state, and it was found that these peaks are due to the existence of a pole of the S-matrix near zero energy.

In addition, we overviewed a fitting analysis incorporating the effects of both the virtual state and the compound nuclear resonance, which are metastable states formed in the initial and final states of neutron scattering, respectively, to estimate the actual contribution of the virtual state [11, 14]. As a result, we found that the effect of the virtual state generates an imaginary part of the scattering length of approximately -1 fm in the absorption of the initial state, and the remainder is generated by the decay of the compound nuclear resonance in the final state.

Needless to say, nuclides corresponding to peaks in the S-wave neutron strength function have the property of strongly absorbing thermal neutrons, and two theories regarding the origin of this phenomenon had been independently proposed by the 1960s: the previously mentioned "zero-energy level · giant resonance theory" [28, 29] and the "compound-nuclear resonance theory" [28, 29]. The giant resonance and the compound nucleus resonance have been unified by the intermediate coupling model, [36], which has been successful in explaining the coarse structure that appears in the excitation function of neutron elastic scattering. However, the relationship be-

tween these theories has remained unclear to date in explaining the phenomenon of strong absorption of thermal neutrons. This reanalysis reinterpreted the zero-energy level · giant resonance in terms of virtual states, and further unified the virtual states and compound-nuclear resonances in terms of scattering lengths, constructing a new picture of neutron absorption. The reanalysis in Refs. [9, 11, 14] explained in this paper has updated the overall picture of neutron absorption reactions for the first time in about 70 years, and this is a noteworthy achievement.

While this article has focused on recent topics related to nuclear structure and thermal neutron scattering, the virtual state may have broad implications for nuclear reaction and structure issues involving S-wave neutrons. Analysis taking virtual states into account will likely become increasingly important in phenomena involving the dynamics of S-wave neutrons. For readers interested in reaction phenomena such as virtual states and resonances and wanting to learn more, we recommend the following textbook, Ref. [37].

7. Acknowledgment

The series of research results on thermal neutron scattering presented here were obtained through research begun as graduation research in the Quantum Many-Body Physics Laboratory at Kansai University in 2022 and continued by volunteers after graduation. One of the author (M. I.) would like to express his gratitude to his graduation research team members: Messers M. Okada, T. Okamoto, T. Terao, Y. Yagi, Y. Yamaguchi, R. Nakamoto, T. Fumimoto, T. Maeda and Miss S. Furusho. In particular, Messers Okada, T. Okamoto, and Y. Yamaguchi continued to work on this research after graduation, and even contributed to the creation of materials for this review article. We would like to express our heartfelt gratitude to them.

Author Contributions: Conceptualization, K.K. and M.I.; methodology, K.K. and M.I.; formal analysis, K.K. and M.I.; writing-original draft preparation, M.I.; writing-review and editing, K.K. and M.I.; supervision, K.K. All authors have read and agreed to the published version of the manuscript.

References

[1] Frisch, D. H. "The total cross sections of carbon and hydrogen for neutrons of energies from 35 to 490 kev." *Physical Review* 70, no. 9 (1946): 589. https://doi.org/10.1103/PhysRev.70.589

[2] Baily, C. D., W. E. Bennett, T. Bergstralh, R. G. Nuckolls, H. T. Richards, and J. H. Williams. "The neutron-proton and neutron-carbon scattering cross sections for fast neutrons." *Physical Review* 70, no. 9 (1946): 583. https://doi.org/10.1103/PhysRev.70.583

[3] Blatt, Y. J. M. and V. F. Weisskopf. *Theoretical Nuclear Physics*. New York: Dover Publications, Inc., Wiley, 1966.

[4] Okabe, S. *Quantum Theory: Motion and Methods Simulation Physics 5 (in Japanese)*. Tokyo: Kindai Kagakusha, 1992.

[5] Shimamura, I. "Kyoumei-sanran-butsuri no kiso (in Japanese)." *Journal of the Atomic Collision Research Society* 2, no. 2 (2005): 3.

[6] Schiff, L. I. *Quantum Mechanics, Third Edition*. Singapore: McGraw-Hill Book Company, 1968.

[7] Sunagawa, S. *Quantum Theory of Scattering (in Japanese)*. Tokyo: Iwanami Zensho, 1977.

[8] Lamarsh, J. R. *Introduction to Nuclear Reactor Theory, Vol. 1*. USA: Addison-Wesley Publishing Company, Inc., 1965.

[9] Yamaguchi, Y., M. Okada, T. Terao, S. Furusho, T. Okamoto, Y. Yagi, T. Fumimoto, T. Maeda, R. Nakamoto, and M. Ito. "Strong absorptions of thermal neutrons caused by virtual states." *Prog. Theor. Exp. Phys.* 2024 (2024): 123D02. https://doi.org/10.1093/ptep/ptae168

[10] Breit, G. and E. P. Wigner. "Capture of slow neutron." *Physical Review* 49 (1936): 519.

[11] Okada, M., Y. Yamaguchi, and M. Ito. "Formulae for enhanced cross sections induced by unusual resonant poles." *Prog. Theor. Exp. Phys.* 2025 (2025): 013D03. https://doi.org/10.1093/ptep/ptae195

[12] Feshbach, H., C. E. Porter, and V. F. Weisskopf. "Model for nuclear reactions with neutrons." *Physical Review* 96 (1954): 448. https://doi.org/10.1103/PhysRev.96.448

[13] Kawai, M. and S. Yoshida. *Nuclear Reaction Theory (in Japanese)*. Tokyo: Asakura Physical System, Asakura Shoten, 2002.

[14] Okada, M., Y. Yamaguchi, and M. Ito. "Origin of complex scattering lengths in thermal neutron scattering: State-of-the-art picture." *Journal of the Physical Society of Japan* 95, no. 2 (2026): 024201. https://doi.org/10.7566/JPSJ.95.024201

[15] Sears, V. F. "Neutron scattering lengths and cross sections." *Neutron News* 3 (2006): 26. https://doi.org/10.1080/10448639208218770

[16] Masui, H., S. Aoyama, T. Myo, and K. Katō. "Study of virtual states in ^{5}He and ^{10}Li with the Jost function method." *Nuclear Physics A* 673 (2000): 207. https://doi.org/10.1016/S0375-9474(00)00148-2

[17] Thompson, I. J. and M. V. Zhukov. "Effects of ^{10}Li virtual states on the structure of ^{11}Li." *Phys. Rev. C* 49 (1994): 1904. https://doi/10.1103/PhysRevC.49.1904

[18] Katō, K., T. Yamada, and K. Ikeda. "Dynamical effects on the 9li-n interaction induced by pauli blocking of the j = 0+ pairing correlation." *Prog. Theor. Phys.* 101 (1999): 119. https://doi.org/10.1143/PTP.101.119

[19] Sagawa, H., B. A. Brown, and H. Esbensen. "Parity inversion in the n=7 isotones and the pairing blocking effect." *Phys. Lett. B* 309 (1993): 1. https://doi/10.1016/0370-2693(93)91493-7

[20] Myo, T., K. Katō, Y. Kikuchi, H. Toki, and K. Ikeda. "Tensor correlation in he and li isotopes based on tensor optimized shell model with unitary correlation operator." *International Journal of Modern Physics A* 24 (2009): 2150. https://doi/10.1142/S0217751X0904573X

[21] Tilley, D., J. Kelley, J. Godwin, D. Millener, J. Purcell, C. Sheu, and H. Weller. "Energy levels of light nuclei a=8,9,10." *Nuclear Physics A* 745 (2004): 155. https://doi.org/10.1016/j.nuclphysa.2004.09.059

[22] Kikuchi, Y., M. Odsuren, T. Myo, and K. Katō. "Photodisintegration cross section of ^{9}Be up to 16 mev in the $\alpha+\alpha+n$ three-body model." *Physical Review C* 93 (2016): 054605. https://doi/10.1103/PhysRevC.93.054605

[23] Odsuren, M., Y. Kikuchi, T. Myo, G. Khuukhenkhuu, H. Masui, and K. Katō. "Virtual-state character of the two-body system in the complex scaling method." *Physical Review C* 95 (2017): 064305. https://doi/10.1103/PhysRevC.95.064305

[24] Arnold, C. W., T. B. Clegg, C. Iliadis, H. J. Karwowski, G. C. Rich, J. R. Tompkins, and C. R. Howell. "Cross-section measurement of ^{9}be$(\gamma,n)^{8}$be and implications for $\alpha+\alpha+n\rightarrow{}^{9}$be in the r process." *Physical Review C* 85 (2012): 044605. https://doi/10.1103/PhysRevC.85.044605

[25] Odsuren, M., Y. Kikuchi, T. Myo, M. Aikawa, and K. Katō. "Virtual-state character of the ^{9}Be $1/2^{+}$ state in the ^{9}Be$(\gamma,n)^{8}$Be reaction." *Physical Review C* 92 (2015): 014322. https://doi.org/10.1103/PhysRevC.92.014322

[26] Utsunomiya, H., S. Katayama, I. Gheorghe, S. Imai, H. Yamaguchi, D. Kahl, Y. Sakaguchi, T. Shima, K. Takahisa, and S. Miyamoto. "Photodisintegration of ^{9}Be through the $1/2^{+}$ state and cluster dipole resonance." *Physical Review C* 92 (2015): 064323. https://doi/10.1103/PhysRevC.92.064323

[27] Odsuren, M., Y. Kikuchi, T. Myo, H. Masui, and K. Katō. "Photodisintegration cross sections for resonant states and virtual states." *Physical Review C* 99 (2019): 034312. https://doi/10.1103/PhysRevC.99.034312

[28] Bohr, A. and B. R. Mottelson. *Nuclear Structure I: Single-Particle Motion*. New York: Benjamin, 1969.

[29] Mughabghab, S. F. *Atlas of Neutron Resonance: Resonance Parameters and Thermal Cross Sections. Z=1-100, 5th Edition*. USA: Elsevier, National Nuclear Data Center Brookhaven National Laboratory Utah, 2006.

[30] Weidenmüller, H. A. "Distribution of partial neutron widths for nuclei close to a maximum of the neutron strength function." *Physical Review Letters* 105 (2010): 232501. https://doi.org/10.1103/PhysRevLett.105.232501

[31] Iwamoto, O., N. Iwamoto, S. Kunieda, F. Minato, S. Nakayama, Y. Abe, K. Tsubakihara, S. Okumura, C. Ishizuka, T. Yoshida, S. Chiba, N. Otuka, J. C. Sublet, H. Iwamoto, K. Yamamoto, Y. Nagaya, K. Tada, C. Konno, N. Matsuda, K. Yokoyama, H. Taninaka, A. Oizumi, M. Fukushima, S. Okita, G. Chiba, S. Sato, M. Ohta, and S. Kwon, "JENDL-5." 2021. https://wwwndc.jaea.go.jp/index.html Nuclear Data Center, Japan Atomic Energy Agency.

[32] Takagi, S., H. Marumori, and M. Kawai. *Genshikakuron (in Japanese)*. Tokyo: Iwanami Shoten, 1978.

[33] Ohno, Y., T. Asami, K. Okamoto, and K. Ideno, "Japanese report to EANDC **1**." 2, 1965.

[34] Begzhanov, R. B., D. A. Gladyshev, S. V. Starodubtsev, and T. Khaidarov. "Interaction cross section of neutrons with Sm^{149} and In^{115} nuclei." *Atomic Energy* 16 (1964): 647. https://doi.org/10.1007/BF01115673

[35] Kawai, M. and Y. Iseri. "Anomalous absorption of neutron partial waves by the nuclear optical potential." *Physical Review C* 31 (1985): 400. https://doi.org/10.1103/PhysRevC.31.400

[36] Lane, A. M., R. G. Thomas, and E. P. Wigner. "Giant resonance interpretation of the nucleon-nucleus interaction." *Physical Review* 98 (1955): 693. https://doi.org/10.1103/PhysRev.98.693

[37] Kukulin, V. I., V. M. Krasnopol'sky, and J. Horacel. *Theory of Resonances*. Dordrecht, Boston, London: Kluwer Academic Publishers, 1989.

Information about authors

Makoto Ito *– Professor, Kansai University, Faculty of Systems Engineering and Science, Osaka, Japan, e-mail: itomk@kansai-u.ac.jp*

Kiyoshi Kato *– Emeritus Professor, Hokkaido University, Graduate School of Science, Sapporo, Japan, e-mail: kato@nucl.sci.hokudai.ac.jp*